Hydrogen Dynamics in Supercritical Water Probed by Neutron Scattering and Computer Simulations

Carla Andreani,[†,‡] Giovanni Romanelli,[*,¶] Alexandra Parmentier,[§] Roberto Senesi,[†,‡] Alexander I. Kolesnikov,[‖] Hsin-Yu Ko,[⊥] Marcos Calegari Andrade,[#] and Roberto Car[#]

†*Università degli Studi di Roma Tor Vergata, Dipartimento di Fisica and NAST Centre, Via della Ricerca Scientifica 1, 00133, Roma, Italy*

‡*CNR-IPCF, Istituto per i Processi Chimico-Fisici del CNR di Messina, Viale F. Stagno dAlcontres 37, 98158 Messina, Italy*

¶*ISIS Facility, Rutherford Appleton Laboratory, Chilton, Didcot, Oxfordshire, OX11 0QX, United Kingdom*

§*INFN - Division of Rome Tor Vergata, via della Ricerca Scientifica 1, 00133, Rome, Italy*

‖*Neutron Scattering Division, Oak Ridge National Laboratory, Oak Ridge, Tennessee 37831, United States of America*

⊥*Department of Chemistry and Chemical Biology Cornell University, United States of America*

#*Princeton University, Princeton, New Jersey 08544, United States of America*

E-mail: giovanni.romanelli@stfc.ac.uk

Abstract

In this work, an investigation of supercritical water is presented combining inelastic and deep inelastic neutron scattering experiments, and molecular dynamics simulations based on a machine-learned potential of *ab-initio* quality. The local hydrogen dynamics is investigated at 250 bar and in the temperature range 553–823 K, covering the evolution from subcritical liquid to supercritical gas-like water. The evolution of libration, bending, and stretching motions in the vibrational density of states is studied, analysing the spectral features by a mode decomposition. Moreover, the hydrogen nuclear momentum distribution is measured, and its anisotropy probed experimentally. It is shown that hydrogen bonds survive up to the higher temperatures investigated, and we discuss our results in the framework of the coupling between intramolecular modes and intermolecular librations. Results show that the local potential affecting hydrogen becomes less anisotropic within the molecular plane in the supercritical phase, and we attribute this result to the presence of more distorted hydrogen bonds.

Graphical TOC Entry

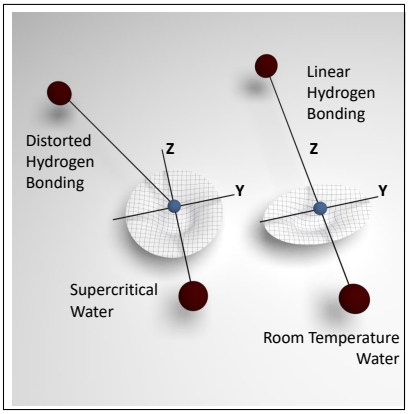

The distorted hydrogen bonds in supercritical water as compared to room-temperature water, and the resulting local potential affecting hydrogen dynamics.

Keywords

Supercritical water; Inelastic neutron scattering; Molecular dynamics; Deep neural network; Hydrogen bonding; Nuclear momentum distribution;

Supercritical water (SCW), *i.e.,* water at temperatures higher than $T_C = 647$ K and pressures higher than $P_C = 221$ bar, has a central role for green and sustainable economies in the treatment of biomass waste,[1] in the production of micro- and nano-particles,[2] as well as in the cooling systems of new-generation power reactors.[3,4] Despite its broad use in industry and engineering, some aspects of its microscopic structure and dynamics are still a matter of debate, and a deeper understanding is needed to improve the efficiency of the use of SCW as an environmentally friendly solvent.[5,6] The ultimate goal for the vast field of SCW-based applications lies in the possibility to modify and tune Hydrogen Bonds (HBs) as a function of the thermodynamic state. The maximum number of HBs per water molecule is considered to be $N_{HB} = 4$ in the solid state.[7] Upon melting, some HBs break ($N_{HB} \simeq 3$–4), and when the temperature increases further, the number of HBs is expected to decrease, with the limiting case of the perfect-gas phase defined as a collection of non-interacting monomers ($N_{HB} = 0$).

Above the critical point (CP), a distinction between liquid and gas phases becomes ambiguous,[8,9] and a number of experimental[10,11] and theoretical studies,[12] of which we give few examples below, contributed to shed light onto the nature of HBs in such thermodynamic range. Early experiments using neutron diffraction[13–16] suggested that the number of HBs was largely reduced at 673 K and 800 bar with respect to Room-Temperature Water (RTW). Raman spectra were reported in Ref.[17] suggesting a gas-like water behavior at pressures in the kbar range yet at temperatures as low as 400 K, in striking disagreement with the proton NMR investigation from Ref.,[18] where still 29% as many HBs at 673 K and 400 bar as for RTW were found. Other authors concluded from Molecular Dynamics (MD) simulations that the most abundant H-bonded species in SCW are dimers,[19] or small clusters composed of $n = 2 - 3$ molecules,[20] while Ref.[21] made a distinction between liquid-like and gas-like SCW based on the Widom line concept.[22] For the two examples they studied,[21] the gas-like SCW arranges in small clusters ($N_{HB} \approx 1.0$), and the liquid-like case can form a single global cluster ($N_{HB} \approx 1.9$). Finally, infra-red spectra from Ref.[23] suggested that the water

structure simplifies to a collection of free monomers only for densities lower than 0.05 g/cm^3. Such distinction (via N_{HB} or cluster size) between liquid-like and gas-like SCW is qualitative and depends on the criteria used to define HBs (see e.g. Ref.[24] for a discussion of HB criteria for RTW).

In this work, we present an experimental and theoretical spectroscopic investigation on SCW, combining Inelastic (INS) and Deep Inelastic Neutron Scattering[25–36] (DINS) experiments, and deep potential MD (DPMD) simulations[37,38] trained with density functional theory (DFT) data. While retaining the accuracy of *ab-initio* MD (AIMD), DPMD simulations are substantially more efficient, allowing for much longer trajectories and larger system sizes than AIMD. This is an important issue when dealing with low-density supercritical water. We have performed experiments at a fixed pressure of 250 bar (higher than P_C) and across a temperature range from 553 K (subcritical liquid), to 823 K (gas-like SCW). As there is no unique definition of the boundary separating liquid- and gas-like phases, Figure S5 in the Supplementary Information (SI) shows the position of the thermodynamic points investigated with respect to the Widom lines at constant heat capacity and thermal compressibility, as well as the locus of constant self-diffusion coefficients. To help understanding the following discussion, we notice that the investigated points at 553 K and 733 K are well within the regions of sub-critical and gas-like SCW, respectively. Neutron scattering is the technique of choice to probe the hydrogen dynamics in condensed-phase systems, owing to the high scattering cross section of protons.[39–41] INS uses thermal neutrons to excite intermolecular and intramolecular vibrational modes (similar to Raman and infra-red spectroscopies yet without selection rules); the measured peaks have been used in the past as fingerprints of the strength of the HB network in water.[16,42,43] DINS makes use of epithermal neutrons,[44] in a scattering regime referred to as Impulse Approximation[45] at high energy and momentum transfers. DINS provides unique information on the single-particle dynamics via the measurement of Nuclear Momentum Distributions (NMDs), thereby accessing the anisotropy and anharmonicity of the local potential affecting nuclei. As neutrons scatter

directly off nuclei, INS and DINS probe local information at the Å- and fraction-of-Å length scales, respectively. Moreover, the high-energy transfer in DINS makes this technique sensitive to the dynamics and structure in the fs time scale.[11,46–50] More details about both experiment and simulation are provided in the SI.

Figure 1 shows the hydrogen-projected Vibrational Densities of States (VDoS), $g(E,T)$, as obtained from our INS measurements performed at the SEQUOIA spectrometer[51] (Spallation Neutron Source, USA). One can notice three main contributions: the libration modes

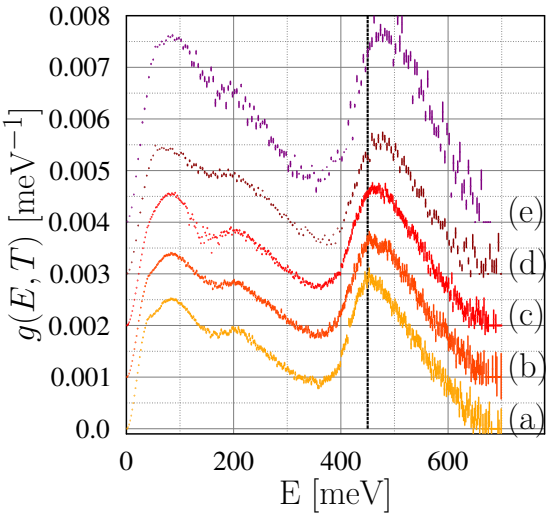

Figure 1: Hydrogen-projected vibrational densities of states under a fixed pressure of 250 bar and at (a) 553 K, (b) 623 K; (c) 663 K; (d) 733 K and (e) 823 K. Spectra have been normalised to unity and successively elevated by 0.001 meV^{-1} to ease the visualisation. A black vertical line is drawn around the stretching vibrational energy to highlight the shift of this mode frequency.

(at energies lower than 100 meV), the bending modes (around 200 meV), and the stretching modes (between 450–473 meV). It is evident how, for increasing temperature and decreasing density, the stretching peak moves to higher frequencies, and the libration peak to lower frequencies. Such opposite trends had already been observed (*e.g.*, upon melting of ice water[52] or in amorphous ices[53]) and are attributed to a weakening of the HB strength. In our study, such HB weakening moves the stretching peak towards the upper limit of the free monomer, on the other side hindered libration modes decrease in frequency towards the free-rotation limit. A more detailed description[20] assumes the overall stretching peak as a superposition of $n = 1$–4 oligomers, and relates the frequency shift to the change in the population of each species, with a trend towards monomers and dimers as temperature increases. We notice

that the presence of quantised librational modes as opposed to stochastic free rotations is a strong suggestion of the presence of intermolecular HBs hindering the molecular reorientation. Quantised rotations for a free water molecule in a C_{60} cage were measured at much lower energies, in the order of few meV.[54] Additional information can be obtained from the broadening of the stretching peak, which we attribute to the coupling between intramolecular OH stretching and intermolecular libration motions.

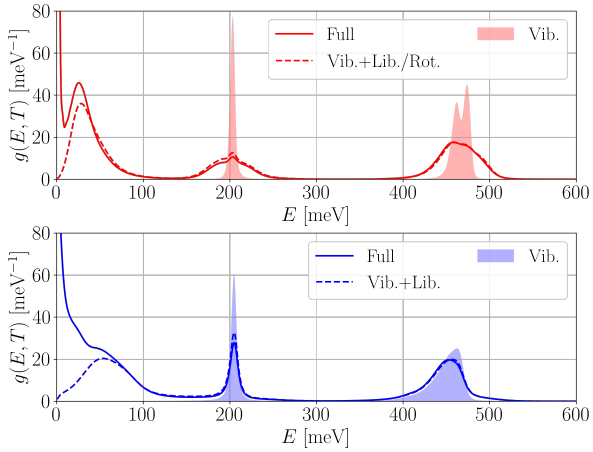

Figure 2: Simulated VDoS of H_2O at experimental subcritical (bottom) and supercritical (top) conditions. For each case, the full spectrum (solid line) is compared with the projected VDoS (dashed line), in which the molecular translations are eliminated. The shaded spectra correspond to intramolecular vibrational spectra (with librational and rotational motions projected out).

To better understand the experimental VDoS, we performed two isobaric–isothermal (NpT) DPMD simulations of water at $P = 250$ bar, at experimental subcritical ($T = 553$ K) and supercritical gas-like conditions ($T = 733$ K), respectively. In these simulations, the interatomic potential was represented by a deep neural network (DNN) trained with DFT energy and forces.[37,38] The DNN receives as input a set of symmetry-preserving local atomic coordinates within a 6 Å smooth radial cutoff, and it outputs the potential energy as a sum of auxiliary "atomic" energies. The DNN potential is herein denoted DP. As shown in several applications,[55,56] DPMD retains the accuracy of AIMD at a much lower computational cost. DFT calculations were performed with the SCAN exchange-correlation functional.[57] SCAN is known to model water more accurately than functionals based on generalized gradient approximations at standard pressure.[58] The DP training procedure followed an active learning scheme proposed by Zhang *et al.*,[59] which consists of iteratively refining a DP model through cycles composed of: exploration, labelling, and training. Exploration consisted of DPMD

simulations of sub and supercritical water at $P = 250$ bar and temperatures $T = 553$ K ($(H_2O)_{32}$), 623 K ($(H_2O)_{32}$), 663 K ($(H_2O)_8$), 733 K ($(H_2O)_8$) and 823 K ($(H_2O)_8$). From these simulations, we selected atomic configurations with large DP error prediction for labelling. The DP error was estimated from the maximum absolute deviation of the forces predicted by 3 independent DPs that differed from each other in the random initialization of the neural network parameters. Labelling consisted of DFT calculations of energy and forces using the SCAN functional. The newly labelled data were appended to the existing training data, and used to further train the DP model. We iteratively refined the model until the DP error estimator was lower than 0.1 eV/Å for all thermodynamic conditions in the exploration step. Our training data contained a total of 3816 and 2300 configurations for systems with $(H_2O)_{32}$ and $(H_2O)_8$, respectively.

The converged DP reproduces the atomic forces of independent AIMD trajectories with a standard deviation lower than 0.063 eV/Å, which is less than 10% of the standard deviation of the AIMD atomic force distribution (see SI for details).

DPMD simulations sampled sub and supercritical water with periodically repeating cells containing 864 and 216 water molecules, respectively. The total DPMD simulation time was 1 ns, with the first 100 ps removed for equilibration. A 0.25 fs time step, required by the fast hydrogen dynamics, was used to numerically integrate the classical equations of motion. The density predicted by DPMD was 0.857 ± 0.003 g/ml at 553 K, and 0.115 ± 0.002 g/ml at 733 K, slightly larger than the corresponding experimental values of 0.78 g/ml and 0.10 g/ml, but consistent with the known performance of the SCAN functional for water at STP, where it predicts a density of 1.05 ± 0.03 g/ml[58] instead of 1.0 g/ml.[60] We notice that the densities predicted by DPMD have much smaller uncertainties but otherwise agree well with the predictions of short SCAN-AIMD trajectories for smaller systems (see SI). DeepMD-kit[61] was used to train the DP models, while Lammps[62] and Quantum ESPRESSO[63] were used to run DPMD simulations and to perform DFT calculations, respectively.

We analysed the structure of the fluid generated by SCAN-based DPMD simulations

at the two thermodynamic points discussed above, *i.e.*, $T = 553$ K, $P = 250$ bar, and $T = 733$ K, $P = 250$ bar. The O–O pair-correlation functions, reported in the SI, show that the fluid at 553 K appears liquid-like while it appears gas-like at 733 K, in agreement with experimental observations reported by Soper and coworkers.[64] To characterize the role played by the HB, we computed the average number of HBs, N_{HB}, according to several criteria commonly used in the literature. We then performed a cluster analysis on the molecules connected by HBs to compute the fraction f_p of molecules percolating between two opposite sides of the simulation cell (see SI for details). While N_{HB} fluctuates between 2.0 and 2.7 in the fluid at 553 K, depending on the HB definition, we found that $N_{HB} \approx 0.4$ for all adopted HB criteria at 733 K. Interestingly, we found that, independently of the HB definition, the fluid at 553 K is always percolating ($f_p = 1$) while it becomes non-percolating ($f_p = 0$) at 733 K, thereby supporting the liquid-like (553 K) and gas-like (733 K) fluid characters. The absence of percolating clusters at 733 K is due to the absence of clusters larger than heptamers in a simulation in which monomers, dimers, and trimers dominate independently of the HB definition.

The changes in the calculated VDoS (Figure 2) from 553 K to 733 K align well with the corresponding changes in the experimental spectra (Figure 1). In particular, both data show a blue shift of the stretching frequency and a red shift of the libration shoulder, while the bending frequency remains mostly unaffected. The spectral changes reflect the aforementioned breakdown of the percolating HB network in water at 733 K characterized by fleeting weak intermolecular HBs and stiff covalent intramolecular bonds. The substantial broadening of the internal-vibration bands at 733 K reflects a strong enhancement of the libration-vibration coupling and the consequent increase of anharmonicity brought in by the higher temperature and the frequent scattering processes among monomers, dimers, and trimers. When comparing the full spectra to the projected VDoS with molecular translations eliminated, we observe that the shoulder associated with librations that merge with the molecular translations at 553 K becomes a more resolved rotational peak at 733 K. Ac-

cording to Ref.[65] nuclear quantum effects, neglected in our simulation, may account for a red shift of the stretching frequency of about 6 meV at 600 K, which is much smaller than the broadening of the peak. The latter originates from the large fluctuation of the local environments and the strong coupling of stretching and libration/rotation modes evident in the DPMD simulations. Finally, multiple scattering contributions at energies below the bending mode can also be expected in the experimental spectra, although mitigated by the low scattering power of the sample. Moreover, it is interesting to notice the splitting of symmetric and antisymmetric stretching modes in the simulated spectra at 733 K, not present at 553 K. Such splitting is particularly evident when librational modes are projected out, and it is possibly hinted in the noisier experimental data.

Table 1: Values of σ_i obtained from a global fit on the DINS spectra. Experimental values (obtained at 250 bar) in the upper part are compared with theoretical predictions from an effective harmonic model (see text) that estimates the proton kinetic energy from the VDoS observed in the INS experiment or in the DPMD simulation (values in parentheses).

Temperature	[K]	553	663	733
Density	[kg/m^3]	777	215	104
DINS Exp				
σ_x	[Å^{-1}]	3.2±0.1	3.5±0.2	3.3±0.5
$\sigma_\perp$	[Å^{-1}]	6.0±0.2	6.0±0.3	6.3±0.6
$\bar{\sigma}$	[Å^{-1}]	5.21±0.03	5.31±0.05	5.44±0.09
$\langle E_K \rangle_x$	[meV]	**21±2**	**26±6**	**23±7**
$\langle E_K \rangle_\perp$	[meV]	**74±9**	**74±14**	**81±14**
$\langle E_K \rangle$	[meV]	**169±3**	**175±3**	**184±3**
Harmonic Model				
$\langle E_K \rangle$	[meV]	**167 (172)**	**178**	**184 (186)**
$\langle E_K \rangle_x$	[meV]	**25 (26)**	**29**	**32 (33)**
$\langle E_K \rangle_y$	[meV]	37 (39)	40	42 (43)
$\langle E_K \rangle_z$	[meV]	105 (107)	109	110 (110)
$\langle E_K \rangle_\perp$	[meV]	**71 (73)**	**75**	**76 (77)**

We augmented the description of the hydrogen dynamics in SCW by performing DINS measurements on the VESUVIO spectrometer (ISIS Facility, UK).[66] The hydrogen NMD,

$n(\vec{p})$, at T = 553 K, 663 K and 733 K was fitted using a multivariate Gaussian function, previously proposed, *e.g.,* in Refs.,[67,68]

$$n(\vec{p}) = \left\langle \prod_{i}^{\{x,y,z\}} \left(2\pi\sigma_i^2\right)^{-\frac{1}{2}} \exp\left(-\frac{p_i^2}{2\sigma_i^2}\right) \right\rangle_{\Omega}, \quad (1)$$

where $\langle \ldots \rangle_{\Omega}$ denotes the angular average of the momentum distribution over molecular orientations due to the disordered nature of the sample.

The multivariate Gaussian model reflects the quasi-harmonic nature of the local potential acting on the proton[69] and is able to capture the anisotropy of the NMD. The index i runs over the three principle axes of the NMD ellipsoid defining a local orthogonal frame centred at the average position of the H atom. σ_i is the root-mean-square H momentum along the i-th direction, corresponding to the i-th component of the nuclear kinetic energy $\langle E_K \rangle_i = \hbar^2\sigma_i^2/2M$, with M the nuclear mass. These components sum up to the total mean kinetic energy, $\langle E_K \rangle = \sum_i \langle E_K \rangle_i$. The total mean kinetic energy can also be estimated from a weighted average of the VDoS spectrum, according to a model proposed by Finkelstein and Moreh,[70,71] which relies on an effective harmonic approximation and decoupling between translation, libration, and internal vibration modes. Interestingly, the total mean kinetic energy estimated in this way, from either the VDoS extracted from INS or the one extracted from DPMD, agrees with the DINS values within experimental errors, as shown in Table 1. While the validity of the quasi-harmonic approximation is supported by DINS, decoupling between internal vibration and libration modes in subcritical and supercritical water is not supported by DPMD simulations. However, since librations weight approximately the same as any of the three independent internal molecular vibrations,[70,71] $\langle E_k \rangle$ is effectively independent of the mixing of librations and vibrations. The best fit of the DINS data is consistent with an oblate NMD ellipsoid with rotational symmetry in the plane of the water molecule. The corresponding principal components of the kinetic energy are $\langle E_k \rangle_{\perp}$ and $\langle E_k \rangle_x$, respectively, where x is a direction perpendicular to the average molecular plane.

Conventionally,[53,72,73] one associates to the water molecules local Cartesian frames in which the z axis is directed along the OH bond, the y axis lies in the plane of the molecule, and the x axis is orthogonal to the molecular plane, as shown in Fig. 3.

Rotational symmetry in the (yz) plane implies $\sigma_y = \sigma_z$, and thus $\langle E_K \rangle_y = \langle E_K \rangle_z = \langle E_K \rangle_\perp$, in contrast with the three-dimensional anisotropy reported for RTW and several forms of ice.[52,53,68,69,72,74] We hypothesize that isotropic H motions in the molecular plane stem from the strong coupling between librations and internal vibrations revealed by DPMD simulations. Librations along x are orthogonal to the H vibrations and do not couple with them. The above interpretation is supported by an extended version of the effective harmonic model that estimates $\langle E_K \rangle_x$, $\langle E_K \rangle_y$, and $\langle E_K \rangle_z$ from the VDoS.[52] The outcome is reported in Table 1. As one can see, the estimate for $\langle E_K \rangle_x$ agrees with the DINS value, whereas the estimates for $\langle E_K \rangle_y$ and $\langle E_K \rangle_z$ do not. In the effective harmonic model $\langle E_K \rangle_z$ originates mostly from the zero-point energy (ZPE) of OH stretching, while $\langle E_K \rangle_y$ is influenced not only by the ZPE of HOH bending but also by ZPE and thermal excitations of intermolecular librations.[52] In this model the libration contribution to stretching, which is prominent in the DPMD simulations, is not present. If one were to assume strong coupling of librations and all the internal modes, as suggested by DPMD, one could obtain $\langle E_K \rangle_\perp \simeq (\langle E_K \rangle_y + \langle E_K \rangle_z)/2$, and the DINS results would be recovered. The key role played by librations is further supported by the following observation. The increase of the total mean kinetic energy with temperature – already measured in a different thermodynamic range near the CP,[10] mainly originates from the thermal excitation of librational overtones, while the stretching modes remain essentially in their vibrational ground state up to the highest temperature of the experiment. In fact, the overall shift of ca. 23 meV on the stretching frequency from 553 K to 823 K corresponds to an increase of only 6 meV in the quasi-harmonic model (*e.g.*, see Eq. 4 in Ref.[72] or Eq. 6 in Ref.[52]). It should be stressed that DINS accesses the anisotropy of the system through the Kurtosis of the neutron Compton profile,[75,76] *i.e.*, the projection of the NMD along the direction of the momentum transfer.[44] From an experimental point

of view, the two cases when the potential is isotropic in the xy or in the yz planes would correspond to values of the Kurtosis that would be different beyond the typical error bars of a DINS experiment.[75,76] The strong coupling between librations and all the internal modes is a consequence of the large anharmonicity present in supercritical water. Taking into account nuclear quantum effects, neglected in our classical MD simulations, should not change the qualitative picture because quantum fluctuations would further enhance the anharmonic coupling.

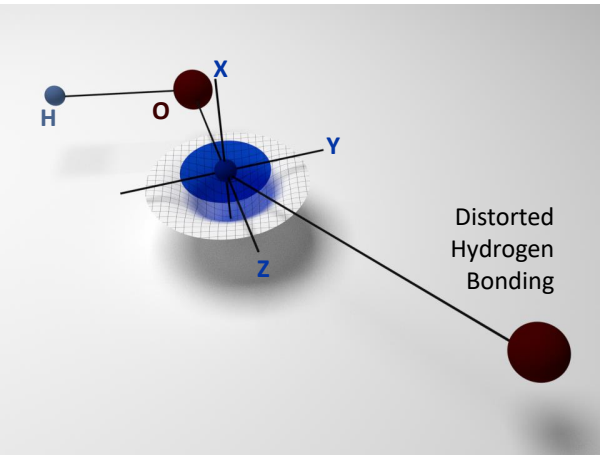

Figure 3: A pictorial representation of the orientation of axes in the interpretation of the hydrogen NMD, and the partially-isotropic local potential and NMD.

Our experimental and theoretical data provided a local picture of SCW in the fs time scale. Our results suggest that i) HBs are still present up to 823 K, 250 bar, and down to 0.078 g/cm^3 (higher than the free-monomer density limit[23] of 0.05 g/cm^3); ii) a strong coupling between intermolecular and intramolecular modes is observed; and iii) the local potential affecting hydrogen and the NMD are symmetric in the molecular plane. Moreover, several studies have suggested that H-bonded species in gas-like SCW mainly comprise water dimers—with highly distorted HBs compared with RTW; for example, it has been shown that pronounced distortions of HBs[77] are quite common, and cyclic dimers, as well as chain-like structures, can also be observed.[78] Consistent with these findings, we also observed larger water oligomers beyond dimers at 733 K. In particular, Figure S3 in the SI shows how HBs, using the Luzar-Chandler definition, are increasingly more distorted when going from RTW to the subcritical and the supercritical phases. This is found to be a robust

trend independent of the adopted HB definition. Moreover, figure S4 in the SI shows that supercritical water contains highly-distorted oligomers, with distortion angles larger than those allowed by the Luzar-Chandler definition, both cyclic and bifurcated in nature. We found these clusters are relevant in reproducing features of the experimentally assigned O–O pair-correlation function (see SI for details). Based on our experiments and simulations, we conclude that the pronounced distortion of HBs in short-living water clusters increases the coupling of intermolecular and intramolecular vibrations and modifies the local potential affecting hydrogen, making it more symmetric in the molecular plane compared with RTW. The fact that our DINS experiment can observe short-living water clusters and helps the understanding of SCW confirms that DINS is a viable technique in measuring local dynamics within the fs time scale.

In conclusions, we have presented new results from INS and DINS experiments on SCW, in a regime where available measurements have relatively large uncertainties due to the challenge in experimental set-up. We have shown how HBs decrease in number while increasing the temperature under constant pressure (250 bar)—a process going from subcritical liquid (553 K) to gas-like SCW (733 K) states (persisting up to 823 K). We have also presented a theoretical VDoS study via DPMD simulations, in which we observe an evident coupling between intramolecular vibrational and intermolecular libration and rotation motions. Our results shed additional light on the challenging dynamics of SCW, thus bringing us one step closer to its comprehensive microscopic understanding.

Acknowledgement

The authors gratefully acknowledge the financial support of Regione Lazio concerning collaboration in scientific research at ISIS@MACH Research Infrastructure (IR approved by Giunta Regionale n. G10795, 7th August 2019 published by BURL n. 69 27th August 2019) and at the ISIS Neutron and Muon Source (UK) of Science and Technology Facilities Coun-

cil (STFC); the financial support of Consiglio Nazionale delle Ricerche within CNR-STFC Agreement 2014-2020 (N 3420), concerning collaboration in scientific research at the ISIS Neutron and Muon Source (UK) of Science and Technology Facilities Council (STFC) is gratefully acknowledged. MFCA, HYK, and RC gratefully acknowledge support from the U.S. Department of Energy (DOE) under Grant No. DE-SC0019394. The work at Spallation Neutron Source was supported by the Scientific User Facility Division, Office of Basic Energy Sciences, (U.S.) Department of Energy (DOE). We thank Prof. C.-K. Loong for very useful discussions. We also thank A. Seel for help during the measurements on the VESUVIO spectrometer; Justin R. Carmichael for the design of the sample container; and John Wenzel, Saad R. Elorfi, and Todd E. Sherline for helping with the experiment on the SEQUOIA spectrometer.

Supporting Information Available: Additional details on the analysis of the experimental data and on the technical aspects of the simulations. This material is available free of charge via the Internet *http://pubs.acs.org*. The entire data used to train the deep neural network potential is publicly available at http://arks.princeton.edu/ark:/88435/dsp01wh246w11p.

References

(1) Correa, C. R.; Kruse, A. Supercritical water gasification of biomass for hydrogen production Review. *The Journal of Supercritical Fluids* **2018**, *133*, 573 – 590.

(2) Fang, Z. *Rapid Production of Micro- and Nano-particles Using Supercritical Water*; Engineering Materials; Springer Berlin Heidelberg, 2010.

(3) Pioro, I. L.; Khan, M.; Hopps, V.; Jacobs, C.; Patkunam, R.; Gopaul, S.; Bakan, K. SCW Pressure-Channel Nuclear Reactor Some Design Features. *Journal of Power and Energy Systems* **2008**, *2*, 874–888.

(4) Oka, Y.; Koshizuka, S.; Ishiwatari, Y.; Yamaji, A. *Super light water reactors and super fast reactors: supercritical-pressure light water cooled reactors*; Springer Science & Business Media, 2010.

(5) Marcus, Y. *Supercritical Water: A Green Solvent: Properties and Uses*; John Wiley & Sons, Hoboken, 2012.

(6) Vogel, G. H. Supercritical Water. A Green Solvent: Properties and Uses. Edited by Yizhak Marcus. *Angewandte Chemie International Edition* **2013**, *52*, 2158–2158.

(7) Daniel, R. M.; Finney, J. L.; Stoneham, M.; Finney, J. L. Water? What's so special about it? *Philosophical Transactions of the Royal Society of London. Series B: Biological Sciences* **2004**, *359*, 1145–1165.

(8) Galli, G.; Pan, D. A closer look at supercritical water. *Proceedings of the National Academy of Sciences* **2013**, *110*, 6250–6251.

(9) Gallo, P.; Corradini, D.; Rovere, M. Widom line and dynamical crossovers as routes to understand supercritical water. *Nature communications* **2014**, *5*, 5806.

(10) Pantalei, C.; Pietropaolo, A.; Senesi, R.; Imberti, S.; Andreani, C.; Mayers, J.; Burnham, C.; Reiter, G. Proton Momentum Distribution of Liquid Water from Room Temperature to the Supercritical Phase. *Physical Review Letters* **2008**, *100*, 177801.

(11) Andreani, C.; Colognesi, D.; Mayers, J.; Reiter, G. F.; Senesi, R. Measurement of momentum distribution of light atoms and molecules in condensed matter systems using inelastic neutron scattering. *Advances in Physics* **2005**, *54*, 377–469.

(12) Morrone, J. A.; Srinivasan, V.; Sebastiani, D.; Car, R. Proton momentum distribution in water: an open path integral molecular dynamics study. *The Journal of Chemical Physics* **2007**, *126*, 234504.

(13) Postorino, P.; Tromp, R.; Ricci, M.; Soper, A.; Neilson, G. The interatomic structure of water at supercritical temperatures. *Nature* **1993**, *366*, 668.

(14) Soper, A. K.; Bruni, F.; Ricci, M. A. Sitesite pair correlation functions of water from 25 to 400C: Revised analysis of new and old diffraction data. *The Journal of Chemical Physics* **1997**, *106*, 247–254.

(15) Andreani, C.; Colognesi, D.; Degiorgi, E.; Ricci, M. A. Proton dynamics in supercritical water. *The Journal of Chemical Physics* **2001**, *115*, 11243–11248.

(16) Ricci, M. A.; Nardone, M.; Fontana, A.; Andreani, C.; Hahn, W. Light and neutron scattering studies of the OH stretching band in liquid and supercritical water. *The Journal of Chemical Physics* **1998**, *108*, 450–454.

(17) Walrafen, G. E.; Chu, Y. C.; Piermarini, G. J. Low-Frequency Raman Scattering from Water at High Pressures and High Temperatures. *The Journal of Physical Chemistry* **1996**, *100*, 10363–10372.

(18) Hoffmann, M. M.; Conradi, M. S. Are There Hydrogen Bonds in Supercritical Water? *Journal of the American Chemical Society* **1997**, *119*, 3811–3817.

(19) Ikushima, Y.; Hatakeda, K.; Saito, N.; Arai, M. An in situ Raman spectroscopy study of subcritical and supercritical water: The peculiarity of hydrogen bonding near the critical point. *The Journal of Chemical Physics* **1998**, *108*, 5855–5860.

(20) Tassaing, T.; Garrain, P. A.; Bgu, D.; Baraille, I. On the cluster composition of supercritical water combining molecular modeling and vibrational spectroscopic data. *The Journal of Chemical Physics* **2010**, *133*, 034103.

(21) Śmiechowski, M.; Schran, C.; Forbert, H.; Marx, D. Correlated Particle Motion and THz Spectral Response of Supercritical Water. *Phys. Rev. Lett.* **2016**, *116*, 027801.

(22) The distinction between a predominantly gas-like and a predominantly liquid-like fluid based on a Widom line is only qualitative because there is no unique thermodynamic definition of a Widom line (see SI).

(23) Tassaing, T.; Danten, Y.; Besnard, M. Infrared spectroscopic study of hydrogen-bonding in water at high temperature and pressure. *Journal of Molecular Liquids* **2002**, *101*, 149 – 158, Molecular Liquids. Water at the New Millenium.

(24) Kumar, R.; Schmidt, J. R.; Skinner, J. L. Hydrogen bonding definitions and dynamics in liquid water. *The Journal of Chemical Physics* **2007**, *126*, 204107.

(25) Gunn, J. M. F.; Andreani, C.; Mayers, J. A new approach to impulsive neutron scattering. *Journal of Physics C: Solid State Physics* **1986**, *19*, L835.

(26) Andreani, C.; Baciocco, G.; Holt, R. S.; Mayers, J. Resolution in deep inelastic neutron scattering using pulsed neutron sources. *Nuclear Instruments and Methods in Physics Research Section A* **1989**, *276*, 297–305.

(27) Mayers, J.; Andreani, C.; Baciocco, G. Initial state effects in deep inelastic neutron scattering. *Phys. Rev. B* **1989**, *39*, 2022–2028.

(28) Andreani, C.; D'Angelo, A.; Gorini, G.; Imberti, S.; Pietropaolo, A.; Rhodes, N. J.; Schooneveld, E. M.; Senesi, R.; Tardocchi, M. CdZnTe γ detector for deep inelastic neutron scattering on the VESUVIO spectrometer. *Applied Physics A: Materials Science & Processing* **2004**, *78*, 903–913.

(29) Mayers, J.; Tomkinson, J.; Abdul-Redah, T.; Stirling, W. G.; Andreani, C.; Senesi, R.; Nardone, M.; Colognesi, D.; Degiorgi, E. VESUVIO-the double difference inverse geometry spectrometer at ISIS. *Physica B Condensed Matter* **2004**, *350*, E659–E662.

(30) Imberti, S.; Andreani, C.; Garbuio, V.; Gorini, G.; Pietropaolo, A.; Senesi, R.; Tardocchi, M. Resolution of the VESUVIO spectrometer for High-energy Inelastic Neutron

Scattering experiments. *Nuclear Instruments and Methods in Physics Research Section A* **2005**, *522*, 463.

(31) Pietropaolo, A.; Andreani, C.; Rebai, M.; Giacomelli, L.; Gorini, G.; Perelli Cippo, E.; Tardocchi, M.; Fazzi, A.; Verona Rinati, G.; Verona, C. et al. Fission diamond detectors for fast-neutron ToF spectroscopy. *Europhys Lett* **2011**, *94*, 62001.

(32) Andreani, C.; Pietropaolo, A.; Senesi, R.; Gorini, G.; Tardocchi, M.; Bracco, A.; Rhodes, N.; Schooneveld, E. Electron-volt spectroscopy at a pulsed neutron source using a resonance detector technique. *Nuclear Instruments and Methods in Physics Research Section A* **2002**, *481*, 509–520.

(33) Schooneveld, E. M.; Mayers, J.; Rhodes, N. J.; Pietropaolo, A.; Andreani, C.; Senesi, R.; Gorini, G.; Perelli-Cippo, E.; Tardocchi, M. Foil cycling technique for the VESUVIO spectrometer operating in the resonance detector configuration. *Review Scientific Instruments* **2006**, *77*, 5103.

(34) Tardocchi, M.; Pietropaolo, A.; Andreani, C.; Bracco, A.; D'Angelo, A.; Gorini, G.; Imberti, S.; Senesi, R.; Rhodes, N. J.; Schooneveld, E. M. Cadmium-Zinc-Telluride photon detector for epithermal neutron spectroscopy-pulse height response characterisation. *Nuclear Instruments and Methods in Physics Research Section A* **2004**, *526*, 477–492.

(35) Pietropaolo, A.; Andreani, C.; Filabozzi, A.; Senesi, R.; Gorini, G.; Perelli-Cippo, E.; Tardocchi, M.; Rhodes, N. J.; Schooneveld, E. M. DINS measurements on VESUVIO in the Resonance Detector configuration: proton mean kinetic energy in water. *Journal of Instrumentation* **2006**, *1*, P04001.

(36) Andreani, C.; Pietropaolo, A.; Senesi, R.; Gorini, G.; Perelli-Cippo, E.; Tardocchi, M.; Rhodes, N.; Schooneveld, E. M. A resonant detector for high-energy inelastic neutron scattering experiments. *Applied Physics Letters* **2004**, *85*, 5454–5456.

(37) Zhang, L.; Han, J.; Wang, H.; Car, R.; E, W. Deep Potential Molecular Dynamics: A Scalable Model with the Accuracy of Quantum Mechanics. *Phys. Rev. Lett.* **2018**, *120*, 143001.

(38) Zhang, L.; Han, J.; Wang, H.; Saidi, W.; Car, R.; E, W. End-to-end symmetry preserving inter-atomic potential energy model for finite and extended systems. *Advances in Neural Information Processing Systems* **2018**, *2018-December*, 4436–4446.

(39) Sears, V. F. Neutron scattering lengths and cross sections. *Neutron News* **1992**, *3*, 26–37.

(40) Andreani, C.; Bosi, P.; Sacchetti, F.; Loong, C. K. Absolute measurements of the stretching mode density of states in polycrystalline ice Ih. *The Journal of Chemical Physics* **1985**, *83*, 750–753.

(41) Pantalei, C.; Senesi, R.; Andreani, C.; Sozzani, P.; Comotti, A.; Bracco, S.; Beretta, M.; Sokol, P. E.; Reiter, G. Interaction of single water molecules with silanols in mesoporous silica. *Physical Chemistry Chemical Physics* **2011**, *13*, 6022–6028.

(42) Senesi, R.; Flammini, D.; Kolesnikov, A. I.; Murray, E. D.; Galli, G.; Andreani, C. The quantum nature of the OH stretching mode in ice and water probed by neutron scattering experiments. *The Journal of Chemical Physics* **2013**, *139*, 074504.

(43) Kolesnikov, A. I.; Reiter, G. F.; Choudhury, N.; Prisk, T. R.; Mamontov, E.; Podlesnyak, A.; Ehlers, G.; Seel, A. G.; Wesolowski, D. J.; Anovitz, L. M. Quantum Tunneling of Water in Beryl: A New State of the Water Molecule. *Phys. Rev. Lett.* **2016**, *116*, 167802.

(44) Andreani, C.; Krzystyniak, M.; Romanelli, G.; Senesi, R.; Fernandez-Alonso, F. Electron-volt neutron spectroscopy: beyond fundamental systems. *Advances in Physics* **2017**, *66*, 1–73.

(45) Sears, V. F. Scaling and final-state interactions in deep-inelastic neutron scattering. *Physical Review B* **1984**, *30*, 44–51.

(46) Andreani, C.; Senesi, R.; Krzystyniak, M.; Romanelli, G.; Fernandez-Alonso, F. In *Neutron Scattering - Applications in Biology, Chemistry, and Materials Science*; Fernandez-Alonso, F., Price, D. L., Eds.; Experimental Methods in the Physical Sciences; Academic Press, 2017; Vol. 49; pp 403 – 457.

(47) Senesi, R.; Romanelli, G.; Adams, M.; Andreani, C. Temperature dependence of the zero point kinetic energy in ice and water above room temperature. *Chemical Physics* **2013**, *427*, 111–116.

(48) Romanelli, G.; Liscio, A.; Senesi, R.; Zamboni, R.; Treossi, E.; Liscio, F.; Giambastiani, G.; Palermo, V.; Fernandez-Alonso, F.; Andreani, C. Soft confinement of water in graphene-oxide membranes. *Carbon* **2016**, *108*, 199–203.

(49) Romanelli, G.; Senesi, R.; Zhang, X.; Loh, K. P.; Andreani, C. Probing the effects of 2D confinement on hydrogen dynamics in water and ice adsorbed in graphene oxide sponges. *Physical Chemistry Chemical Physics* **2015**, *17*, 31680–31684.

(50) Senesi, R.; Kolesnikov, A. I.; Andreani, C. Measurement of proton momentum distributions using a direct geometry instrument. *Journal of Physics: Conference Series* **2014**, *571*, 012007.

(51) Granroth, G. E.; Kolesnikov, A. I.; Sherline, T. E.; Clancy, J. P.; Ross, K. A.; Ruff, J. P. C.; Gaulin, B. D.; Nagler, S. E. SEQUOIA: A Newly Operating Chopper Spectrometer at the SNS. *Journal of Physics: Conference Series* **2010**, *251*, 012058.

(52) Andreani, C.; Romanelli, G.; Senesi, R. A combined INS and DINS study of proton quantum dynamics of ice and water across the triple point and in the supercritical phase. *Chemical Physics* **2013**, *427*, 106–110.

(53) Parmentier, A.; Shephard, J. J.; Romanelli, G.; Senesi, R.; Salzmann, C. G.; Andreani, C. Evolution of Hydrogen Dynamics in Amorphous Ice with Density. *The Journal of Physical Chemistry Letters* **2015**, *6*, 2038–2042.

(54) Beduz, C.; Carravetta, M.; Chen, J. Y.-C.; Concistrè, M.; Denning, M.; Frunzi, M.; Horsewill, A. J.; Johannessen, O. G.; Lawler, R.; Lei, X. et al. Quantum rotation of ortho and para-water encapsulated in a fullerene cage. *Proceedings of the National Academy of Sciences* **2012**, *109*, 12894–12898.

(55) Calegari Andrade, M. F.; Ko, H.-Y.; Zhang, L.; Car, R.; Selloni, A. Free energy of proton transfer at the water–TiO2 interface from ab initio deep potential molecular dynamics. *Chem. Sci.* **2020**, *11*, 2335–2341.

(56) Niu, H.; Bonati, L.; Piaggi, P. M.; Parrinello, M. Ab initio phase diagram and nucleation of gallium. *Nature communications* **2020**, *11*, 2654.

(57) Sun, J.; Ruzsinszky, A.; Perdew, J. P. Strongly Constrained and Appropriately Normed Semilocal Density Functional. *Phys. Rev. Lett.* **2015**, *115*, 036402.

(58) Chen, M.; Ko, H.-Y.; Remsing, R. C.; Andrade, M. F. C.; Santra, B.; Sun, Z.; Selloni, A.; Car, R.; Klein, M. L.; Perdew, J. P. et al. Ab initio theory and modeling of water. *Proc. Natl. Acad. Sci. U.S.A.* **2017**, *114*, 10846–10851.

(59) Zhang, L.; Lin, D.-Y.; Wang, H.; Car, R.; E, W. Active learning of uniformly accurate interatomic potentials for materials simulation. *Phys. Rev. Materials* **2019**, *3*, 023804.

(60) Haynes, W. Handbook of Chemistry and Physics, CRC. *Taylor and Francis Group: Boca Raton, FL* **2015**, *2016*, 3–82.

(61) Wang, H.; Zhang, L.; Han, J.; E, W. DeePMD-kit: A deep learning package for many-body potential energy representation and molecular dynamics. *Computer Physics Communications* **2018**, *228*, 178 – 184.

(62) Plimpton, S. Fast Parallel Algorithms for Short-Range Molecular Dynamics. *Journal of Computational Physics* **1995**, *117*, 1 – 19.

(63) Giannozzi, P.; Baroni, S.; Bonini, N.; Calandra, M.; Car, R.; Cavazzoni, C.; Ceresoli, D.; Chiarotti, G. L.; Cococcioni, M.; Dabo, I. et al. QUANTUM ESPRESSO: a modular and open-source software project for quantum simulations of materials. *J. Phys.: Condens. Matter* **2009**, *21*, 395502.

(64) Bernabei, M.; Botti, A.; Bruni, F.; Ricci, M. A.; Soper, A. K. Percolation and three-dimensional structure of supercritical water. *Phys. Rev. E* **2008**, *78*, 021505.

(65) Rossi, M.; Liu, H.; Paesani, F.; Bowman, J.; Ceriotti, M. Communication: On the consistency of approximate quantum dynamics simulation methods for vibrational spectra in the condensed phase. *The Journal of Chemical Physics* **2014**, *141*, 181101.

(66) Romanelli, G.; Krzystyniak, M.; Senesi, R.; Raspino, D.; Boxall, J.; Pooley, D.; Moorby, S.; Schooneveld, E.; Rhodes, N. J.; Andreani, C. et al. Characterisation of the incident beam and current diffraction capabilities on the VESUVIO spectrometer. *Measurement Science and Technology* **2017**, *28*, 095501.

(67) Flammini, D.; Pietropaolo, A.; Senesi, R.; Andreani, C.; McBride, F.; Hodgson, A.; Adams, M. A.; Lin, L.; Car, R. Spherical momentum distribution of the protons in hexagonal ice from modeling of inelastic neutron scattering data . *The Journal of Chemical Physics* **2012**, *136*, 024504.

(68) Romanelli, G.; Ceriotti, M.; Manolopoulos, D. E.; Pantalei, C.; Senesi, R.; Andreani, C. Direct Measurement of Competing Quantum Effects on the Kinetic Energy of Heavy Water upon Melting. *The Journal of Physical Chemistry Letters* **2013**, *4*, 3251–3256.

(69) Lin, L.; Morrone, J. A.; Car, R.; Parrinello, M. Momentum distribution, vibrational dynamics, and the potential of mean force in ice. *Physical Review B* **2011**, *83*, 220302.

(70) Moreh, R.; Sellyey, W. C.; Sutton, D.; Vodhanel, R. Widths of the 6.92 and 7.12 MeV levels in ^{16}O and the influence of the effective temperature. *Physical Review C* **1985**, *31*, 2314–2316.

(71) Finkelstein, Y.; Moreh, R. Temperature dependence of the proton kinetic energy in water between 5 and 673 K. *Chemical Physics* **2014**, *431*, 58–63.

(72) Romanelli, G.; Fernandez-Alonso, F.; Andreani, C. The Harmonic Picture of Nuclear Mean Kinetic Energies in Heavy Water. *Journal of Physics: Conference Series* **2014**, *571*, 012003.

(73) Romanelli, G. *On the Quantum Contributions to the Phase Transitions in Water Probed by Inelastic Neutron Scattering*; Ph.D Thesis - Universitá degli Studi di Roma "Tor Vergata", 2015.

(74) Andreani, C.; Romanelli, G.; Senesi, R. Direct Measurements of Quantum Kinetic Energy Tensor in Stable and Metastable Water near the Triple Point: An Experimental Benchmark. *The Journal of Physical Chemistry Letters* **2016**, *7*, 2216–2220.

(75) Romanelli, G.; Krzystyniak, M. On the line-shape analysis of Compton profiles and its application to neutron scattering. *Nuclear Instruments and Methods in Physics Research Section A* **2016**, *819*, 84 – 88.

(76) Krzystyniak, M.; Romanelli, G.; Drużbicki, K.; Tolchenov, R.; Gigg, M.; Hewer, B.; Fernandez-Alonso, F. Model selection in neutron Compton scattering - a Bayesian approach with physical constraints. *Journal of Physics: Conference Series* **2018**, *1055*, 012012.

(77) Wernet, P.; Testemale, D.; Hazemann, J.-L.; Argoud, R.; Glatzel, P.; Pettersson, L. G. M.; Nilsson, A.; Bergmann, U. Spectroscopic characterization of microscopic hydrogen-bonding disparities in supercritical water. *The Journal of Chemical Physics* **2005**, *123*, 154503.

(78) Boero, M.; Terakura, K.; Ikeshoji, T.; Liew, C. C.; Parrinello, M. Hydrogen Bonding and Dipole Moment of Water at Supercritical Conditions: A First-Principles Molecular Dynamics Study. *Physical Review Letters* **2000**, *85*, 3245–3248.